PERGAMON

International Journal of Plasticity
16 (2000) 1345–1369

INTERNATIONAL JOURNAL OF
Plasticity

www.elsevier.com/locate/ijplas

A multivariant micromechanical model for SMAs Part 1. Crystallographic issues for single crystal model

Xiujie Gao *, Miinshiou Huang, L. Catherine Brinson

Department of Mechanical Engineering, Northwestern University, Evanston, IL 60208, USA

Received in final revised form 18 January 2000

Abstract

A general 3-D multivariant model for shape memory alloy constitutive behavior is further developed in this paper. The model is based on the habit planes and transformation directions for variants of martensite and uses a thermodynamic and micromechanics approach to develop the governing equations for thermomechanical response. The model accounts for the self-accommodating group structure exhibited during martensitic plate formation and utilizes this concept in its calculation of the interaction energy between variants. In this paper, we expand the multivariant model to consider the impact of inclusion shape on model predictions. A direction selection scheme is proposed for penny shaped inclusions and is based on the fact that several habit plane variants tend to cluster about one of the {011} or {001} poles. We also explore in detail the crystallographic basis of material response and the impact of specific crystallographic changes on the macroscopic single crystal constitutive response. Differences between type I and type II twinning are examined and it is shown that choice of the proper twinning type is essential to capture experimental data. The grouping structure is examined and several different options published for a NiTi alloy are implemented and results compared. Several concepts, i.e. artificial merging, exclusive and non-exclusive grouping, are raised to assist exploration of NiTi grouping possibilities. The anisotropy of the single crystal material response is illustrated and implications on higher level modeling are discussed. It is noted that properly representing the details of the crystallographic microstructure is crucial to obtaining accurate macroscopic stress–strain predictions. © 2000 Elsevier Science Ltd. All rights reserved.

Keywords: A. Microstructures; A. Phase-transformation; A. Thermomechanical processes; A. Twinning; B. Constitutive behaviour

* Corresponding author.

0749-6419/00/$ - see front matter © 2000 Elsevier Science Ltd. All rights reserved.
PII: S0749-6419(00)00013-9

1. Introduction

In a previous paper (Huang and Brinson, 1998), a multivariant micromechanics model for shape memory alloy (SMA) response prediction was developed. While several other micromechanics based constitutive models have been explored recently (Patoor et al., 1994; Lexcellent et al., 1996; Lu and Weng, 1997, 1998), the multivariant model is unique in its representation of the grouping structure of martensite. We recognize that martensitic variants tend to form in self-accomodated groups to minimize the energy associated with their formation and we explicitly account for this in calculation of the interaction energy based on groups of variants.

In the initial work on the multivariant model, however, many details of the crystallographic modeling were left unexplored. In further work with the model, in particular in comparison to experimental data, we have discovered that many of these issues must be dealt with for accurate characterization. In this paper, we will consider the impact of several microscale characteristics on macroscale response. First, since the original model utilized only spherical inclusions to represent the martensitic variants, we examine the impact of plate-like inclusion shapes on the overall response. The advantage of the spherical inclusion, in spite of its obvious drawbacks, was the symmetry: with the choice of penny-shaped inclusions, directionality of the inclusion must also be chosen consistently with the transformation features for realistic modeling.

We also examine more rigorously the nature of the variant formation. We discuss the nature of 2H, 3R and 18R martensitic variant structure and the changes required for the grouping structure in the micromechanics model. The distinction between type I and type II twins are summarized and it is shown to be important to use the proper twinning type and associated parameters for accurate data characterization. The anisotropy of the single crystal material is highlighted and results will be shown which suggest further change to the model to account for the modulus anisotropy may be essential. Finally, for a B19′ material, NiTi, several variant grouping possibilities published in the literature are explored and the differences in macroscopic model predictions are shown. Other issues will be raised, but left as targets for further work, such as including correspondence variants in the model, and how to handle the non-invariant plane products seen in recent experiments on CuAlNi.

2. Background

In this section, basic background information on martensitic variant formation in shape memory alloys will be highlighted with an emphasis on the essential features of the crystallography which need to be reflected properly in the multivariant model. This is not intended to be an exhaustive review of variant formation, but rather an overview to assist in understanding the issues of concern for proper constitutive modeling. The reader is referred to the cited references for greater detail on the issues raised.

2.1. Habit plane variant vs. correspondence variant

Given a fixed oriented single crystal of the austenite, many differently oriented martensite single crystals can form by cooling, each with a unique lattice correspondence relative to the parent phase. These are termed "correspondence variant" (CV). The habit plane is the undistorted plane of interface between the austenite and martensite phases in martensitic transformation. Many habit planes with different orientations can be observed during the A $\Longleftrightarrow$ M transformation. Near each habit plane, the transformation strain of the martensite can be treated as an invariant plane strain on that habit plane, and thus the martensite above the habit plane is called a "habit plane variant" (HPV).

Although habit plane variants are often used for description of thermally transformed martensite, in fact habit plane variants are often composed of smaller correspondence variants subunits. When describing deformation behavior of martensite it is necessary to work with correspondence variants since upon loading the final crystallographic structure is a single crystal of the CV most favorably oriented to the applied load (Saburi and Nenno, 1981). Different long-period stacking order structures for martensites, for example 2H, 3R, 9R and 18R, have different relationships between the correspondence variant and habit plane variant (Saburi and Nenno, 1981).

Among all shape memory alloys in which thermoelastic martensitic transformation occur, the parent phases have ordered BCC (B2 type or $D0_3$ type) structures (Funakubo, 1987). The martensitic transformation in these alloys occurs by deformation of the {110} planes into planes with hexagonal or rhombohedral symmetry and arrangement into long-period stacking order martensitic phase. The notations such as 2H, 18R etc. are Ramsdel notation (Funakubo, 1987; Otsuka et al., 1993) where the numbers here represent the number of the basal plane layers (planes distorted from parent {110} type plane) in one period. A period is one that contains least number of layers necessary to form an orthorhombic unit cell of the martensitic phase. R represents rhombohedral symmetry and H represents hexagonal symmetry in the direction vertical to the basal plane when ordering of atoms is disregarded. Some intricacies and inconsistencies in martensite notation are discussed in the literature (Otsuka et al., 1993). Note that B2, $D0_3$, and $B19'$ are Strukturbericht (Barrett and Massalski, 1980) notation and prime indicates martensite phase.

In martensite with an 18R (or 9R) structure (for example, CuZnAl and CuZnGa SMAs), there are 12 correspondence variants. By calculating using phenomenological crystallographic theories (Wechsler et al., 1953; Bowles and Machenzie, 1954; Saburi et al., 1976), each of them leads to two crystallographically equivalent habit plane variants with stacking faults acting as the invariant plane shear. Thus there are 24 habit plane variants in 18R (or 9R) martensite. Note that a habit plane variant in the 18R (or 9R) martensite is not only a single crystal but also a correspondence variant. The crystallographic relation between the four habit plane variants in the $(01\bar{1})$ plate group for 18R (or 9R) structure is shown in Fig. 1.

In martensite with an orthorhombic 2H structure (for example γ_1' CuAlNi and γ_2''Au–Cd), there are six correspondence variants. A habit plane variant in this case is composed of two different correspondence variants which are in a twin relation. The

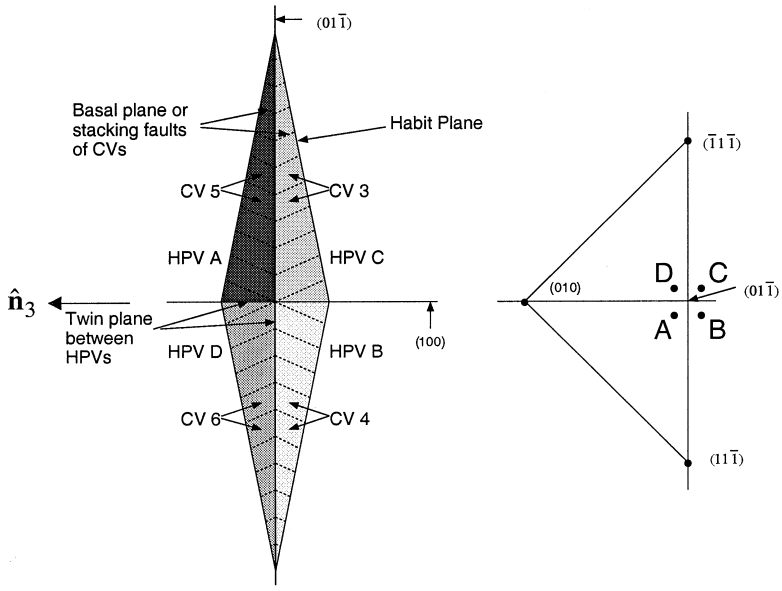

Fig. 1. Crystallographic relations between the four martensitic habit plane variants in the $(01\bar{1})_{\beta_1}$ plate group for 18R (9R) martensite (after Saburi and Wayman, 1979).

six correspondence variants can be divided into three groups according to the condition that the two correspondence variants in a same group have a common contraction direction during the Bain distortion. Since one specific CV can only form twins with CVs not in the same group, there are 12 possible pairs of CVs which could form twins. In addition, each CV of the pair can assume a large or small relative volume fraction with respect to the other in the pair, which again leads to 24 HPVs. The geometry of the $(01\bar{1})$ plate group for orthorhombic 2H martensite is shown in Fig. 2. Note that each habit plane variant here is neither a single correspondence variant nor a single crystal (due to the different lattice orientations of the two CVs).

In martensite with a 3R structure (for example Ni–Al), there are three correspondence variants. A habit plane variant in this case is again composed of two different correspondence variants which are in a twin relation. In this case, each CV can form twins with other CVs, and thus there are three possible pairs. Each pair can form twins with respect to two different twinning planes and two cystallographically equivalent solutions for the HP are possible for a specific pair and a specific twinning plane. This leads to 12 possibilities for HPs. As in the case of 2H, the two CVs in the pair also have a major and minor component which finally brings us 24 HPVs again. The geometry of the $(01\bar{1})$ plate group for 3R martensite is shown in Fig. 3. Note again that each habit plane variant here is neither a correspondence variant nor a single crystal.

It is worth noting that there are always 24 HPVs in the martensitic transformation regardless the type of long-period stacking order structure: this result occurs because given three different numbers for the components of the habit plane normal, there are always 24 crystallographically equivalent HPNs. How to make these HP appear,

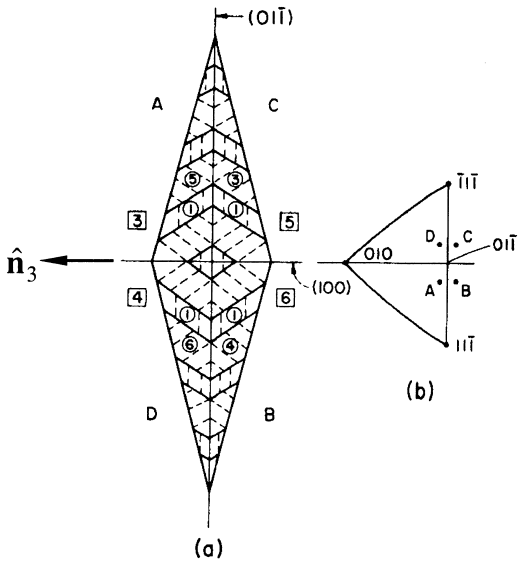

Fig. 2. (a) Geometry of (01$\bar{1}$) plate group for 2H martensite. Solid line: twin boundaries and boundaries between variants. Dashed line: basal planes. (b) Habit plane normals of the variants in (a) in a (01$\bar{1}$) standard projection (after Saburi and Wayman, 1979).

either by having stacking faults in a CV (in 9R or18R) or by forming twins among two CVs (2H or 3R) is a separate issue. The above description of martensitic grouping pertains to thermally induced martensite. As mentioned before, the deformation product eventually attained under loading is a single crystal of the correspondence variant which is most favorably oriented with respect to the applied stress and the recoverable deformation in the shape memory effect occurs by reorientation of these minimum subunits characterized by the lattice correspondence. Therefore, the micromechanical models simply using 24 habit plane variants may not be appropriate in some cases.

The multivariant model is currently developed to handle natural variant grouping structures such as that illustrated by 18R martensites, where each HPV is also a CV. In the later summary of the Multivariant model, this issue will be raised again and we will mention how extension to structures such as the 2H and 3R can be made. It will be important to bear in mind the striking difference between the different martensitic structures at the microscopic level.

2.2. *Type I Twinning vs. Type II Twinning*

Deformation twins can be classified into three types according to the rationality of K_1, K_2, η_1 and η_2 (Reed-Hill and Abbzachian, 1992):

1. Type I twin (a twin of the first kind) when K_1 is a rational plane and η_2 is a rational direction.

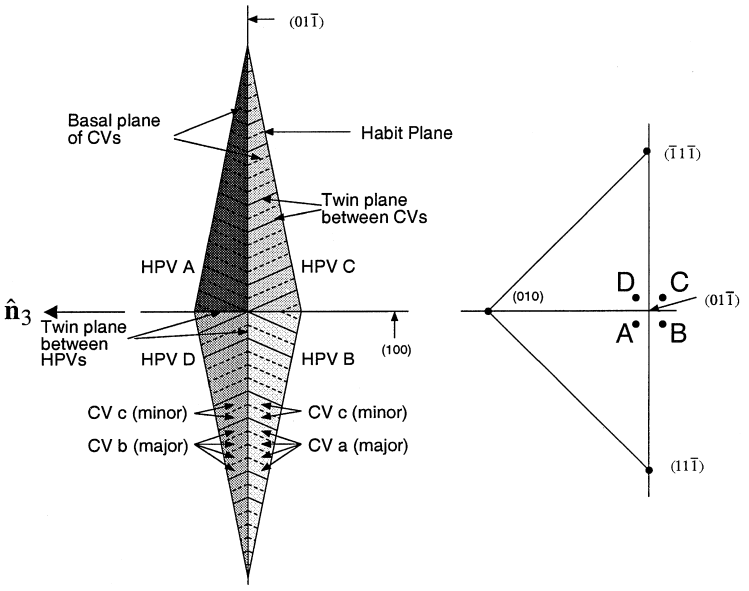

Fig. 3. Crystallographic relations between the four martensitic habit plane variants in the $(01\bar{1})_{\beta_1}$ plate group for 3R martensite (after Saburi and Wayman, 1979).

2. Type II twin (a twin of the second kind) when K_2 is a rational plane and η_1 is a rational direction.
3. A compound twin when all four elements K_1, K_2, η_1 and η_2 are rational.

K_1 and K_2 are the first and the second undistorted plane respectively. η_1 is the shear direction and η_2 is the intersection of the plane of shear with the second undistorted plane, i.e. K_2.

During the implementation of the phenomenological crystallographic theories (Wechsler et al., 1953; Bowles and Machenzie, 1954; Saburi et al., 1976), the twinning plane has been assumed to originate from one of the $\{110\}_P$ planes in the parent phase, and thus the twinning type is type I because of the rationality of this $\{110\}_P$ type plane. While most of the known twinning types are type I (Wechsler et al., 1953; Crocker, 1965), type II twinning is also always possible if type I twinning can form (Bilby and Crocker, 1965) because they are reciprocal to each other. Moreover, some type II twins have been found in many kinds of materials (Cahn, 1953; Knowles and Smith, 1981; Okamoto et al., 1986; Matsumoto et al., 1987).

In these SMAs mentioned above, some have a 2H long-period stacking order structure, for instance, the $\beta_1 \rightarrow \gamma_1'$ CuAlNi martensitic transformation, in which twinning plays a very important role as an invariant plane shear. Although most of the crystallographic parameters calculated using type I twinning are close to those calculated using type II, the results from type II are even closer to the experimental results, especially resolving the inconsistency on the K_1 plane normal relative to the parent lattice.

These observations urge further study of the transformation mechanism in other alloys because the type of twinning imposes very important influence on the crystallographic parameters, which are critical for all micromechanical models of martensitic transformation. It also may have some influence on the geometry of the plate groups in these SMAs and the conversion process.

Illustrating the importance of understanding and correctly capturing the crystallographic details in a micromechanical model, note that a comparison of our model to experimental data using type I and type II twinning produced greatly different results. When we used type II twinning, which is the prefered one by the material, the results corresponded to the experimental results very well (see later section in this paper).

2.3. Invariant plane vs. non-invariant plane

So far, almost all theoretical models assumed the interface between austenite and martensite is an invariant plane, i.e. habit plane. Upon this assumption, all kinds of crystallographic theories of martensitic transformation yield the same habit plane normals and the magnitude and direction of the invariant plane shear (IPS). However, recent experimental results on the deformation field of single crystal Cu–13.7Ni–4.18Al (wt.%) SMA by using Moiré interference technique (Sun et al., 1997; Sun et al., 1999) identify two kinds of A–M interfaces with different deformation features, i.e. invariant plane (IP) and non-invariant plane (NIP). The experiment demonstrates that the invariant plane assumption on the A–M interface agrees very well with the Moiré measurement in the temperature range of shape memory effect but does not hold in the case of superelasticity at high temperature.

The experiments clearly show a highly distorted strain field around the interface for superelasticity case, although the angle of the A–M interface is the same as that predicted by the phenomenological theory. While no attempt is made in this paper to address non-invariant plane martensitic deformation theory, we want to raise this issue as a significant concern for future work with this and other micromechanical models for SMA behavior.

3. Model

In this section, we first review the multivariant model as presented in our previous work (Huang and Brinson, 1998), then extend the model to accommodate different inclusion shapes. The model is based on a combined thermodynamic and micromechanics approach and yields a set of equations which are solved numerically for the evolution of the martensite fraction of each variant. A key component in the development and success of the model is the formation of groups of variants, which represent the tendency of the martensite plates in the real material to form in self-accommodated groups to minimize the energy.

The model was demonstrated with classical uniaxial loading and thermal loading tests for both a simplified (idealized) two-variant SMA and a 24-variant SMA with crystallographic material parameters taken from the literature. Temperature induced

transformations, shape memory effect, pseudoelasticity and ferroelasticity are all accounted for properly by the model. In the two-variant case, perfectly and imperfectly self-accommodated variants were considered to illustrate several features of the model. In addition to the uniaxial loading cases, a biaxial loading case was also simulated and the results were compared qualitatively to experimental data from the literature. The results from the simulation are in good qualitative agreement with the data.

3.1. Summary of single crystal model

The multivariant model begins with the complementary free energy of the material

$$\Psi(\Sigma_{ij}, T, f^n) = -[\Delta G_{\text{ch}} + W_{\text{mech}} + W_{\text{sur}} - \Sigma_{ij}E_{ij}] \tag{1}$$

the rate of change of which is set equal to the rate of change of the dissipation energy

$$\mathrm{d}\Psi|_{\Sigma_{ij},T} = \mathrm{d}W^{\text{d}} \geqslant 0 \tag{2}$$

For the chemical free energy, ΔG_{ch}, a standard expression is used, linearly proportional to temperature change; the surface energy, W_{sur}, is small in comparison to other terms and is neglected. The mechanical energy, W_{mech}, is approximated by a micromechanics technique in which the formation of martensitic variants in a shape memory alloy under loading is viewed as a superposition of the external loading acting on a homogeneous material and a set of transforming inclusions. With this approach it can be shown that the mechanical energy reduces to a stored elastic energy term plus an interaction energy term, E_{int},

$$W_{\text{mech}} = \frac{1}{2V}\int_V \sigma_{ij}\varepsilon_{ij}^{\text{e}}\mathrm{d}V = \frac{1}{2}\Sigma_{ij}C_{ijkl}^{-1}\Sigma_{kl} - \underbrace{\frac{1}{2V}\int_V \sigma_{ij}^{\text{II}}\varepsilon_{ij}^{\text{tr}}\mathrm{d}V}_{E_{\text{int}}} \tag{3}$$

where Σ_{ij} is the macroscopic applied stress, σ_{ij}, ε_{ij} are the local stress and strain (superscripts e and tr on the strain represent elastic and transformation strains respectively), and C_{ijkl} is the modulus of the material. In order to use closed form expression of Eshely Tensor in the subsequent Eshelby inclusion analysis (Mura, 1987), C_{ijkl} will be taken to be isotropic and identical moduli for austenite and martensite are used.

To calculate the interaction energy, it was essential to recognize that the martensitic variants tend to form in self-accommodated groups of compatible variants in order to minimize the energy of their formation (see Figs. 1–4). Using this key concept, the interaction energy is approximated as a sum over G groups of M self-accommodating variants each

$$E_{\text{int}} = -\frac{1}{2V}\int_V \sigma_{ij}^{\text{II}}\varepsilon_{ij}^{\text{tr}}\mathrm{d}V = -\frac{1}{2}\sum_{g=1}^{G}\langle\sigma_{ij}\rangle^{\text{g}}\bar{\varepsilon}_{ij}^{g}\bar{f}^{g} \tag{4}$$

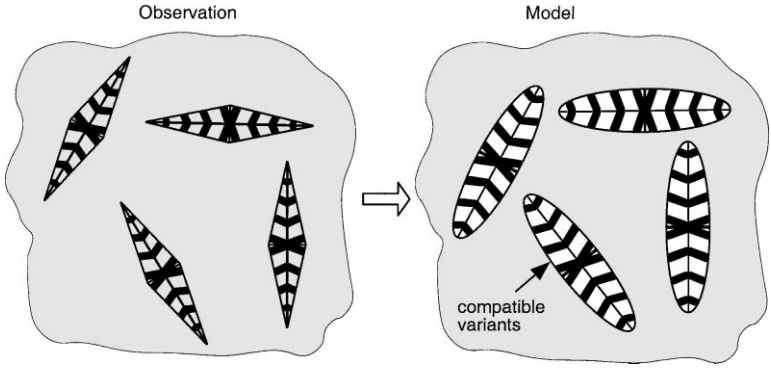

Fig. 4. Model represents variants growing in the matrix: each inclusion is a group of compatible variants that grow together to minimize the energy of their formation. Here a self-accommodating group is depicted with a diamond shape (Saburi and Wayman, 1979); it is noted that parallelogram (Murakami et al., 1994) and triangular shapes (Miyazaki et al., 1989a,b) have also been proposed for various shape memory alloys.

where $\langle\sigma_{ij}\rangle^g$, $\bar{\varepsilon}^g_{ij}$, $\bar{f}^g$ are the average stress in an inclusion of group g, average transformation strain of group g and the volume fraction of group g. The transformation strain of each variant, ε^n_{ij} ($n=1,2,\ldots,G\times M$), is calculated from the basic crystallographic information on the habit plane normal, **n**, invariant plane shear direction, **m**, and magnitude of the invariant plane shear, g, for a given material [Eq. 10]. Eq. 4 can be shown to reduce to

$$E_{\text{int}} = -\frac{1}{2}\sum_{g=1}^{G}\bar{\varepsilon}^g_{ij}\left(\hat{\sigma}^g_{ij} - \sum_{m=1}^{G}\bar{f}^m\hat{\sigma}^m_{ij}\right)\bar{f}^g \tag{5}$$

where

$$\hat{\sigma}^g_{ij} = C_{ijkl}\left(S^g_{klmn}\bar{\varepsilon}^g_{mn} - \bar{\varepsilon}^g_{kl}\right) \tag{6}$$

and S^g_{ijkl} is the Eshelby tensor of group g.

The final system of equations obtained from (2) can be written in vector form for the evolution of volume fraction **f** as

$$\mathbf{F}^d\dot{\mathbf{f}} = \mathbf{F}_{\text{ext}} + \mathbf{F}_{\text{int}} + \mathbf{F}_{\text{wall}} - \mathbf{F}_{\text{fric}} \tag{7}$$

where each vector has N components representing each of the $N=G\times M$ variants. The external driving force on the system for the nth variant is determined from the applied stress and temperature

$$F^n_{\text{ext}} = -B(T - T_0) + \Sigma_{ij}\varepsilon^n_{ij} \tag{8}$$

where B is a linearized factor of difference in the chemical free energies per unit volume of the two phases near the thermodynamic equilibrium temperature T_0. The interaction force is the gradient of the interaction energy

$$F^n_{\text{int}} = -\frac{\partial E_{\text{int}}}{\partial f^n} \tag{9}$$

F_{wall} represents a boundary force applied on the system to keep the martensite fraction within physical bounds ($0 \leqslant f^n \leqslant 1$), and it only appears for a variant when the volume fraction of that variant is very close to 0 or 1. A combined elastic wall and neutral zone model was employed in the calculation. Both width of elastic wall and the neutral zone are taken to be 10^{-5} (Huang, 1997). F^n_{fric} is a constant F^{C} if variant n is actively transforming forward, and $-F^{\text{C}}$ when transforming backward. The system of Eq. (7) can be solved numerically. Note that the formulation of the interaction energy imposes that an "inclusion" is a group of variants; at the same time, however, the volume fractions for each individual variant are tracked so that a final product of a single variant is possible.

With the grouping structure as represented by Eqs. (4) and (5) the final product that forms can be either a single variant or a single group or variants from several groups, depending on the thermomechanical forces applied to the system. Since there is only one level to the grouping structure, the model is appropriately configured for representation of 18R (or 9R) martensitic structures, where there are six groups of four habit plane variants that form naturally under cooling and where each HPV is also a CV so that the deformation products that form under load are properly accounted for. Thus, in a CuZnAl (18R or 9R) SMA, since each habit plane variant is a correspondence variant, our current model is appropriate. However, for materials such as CuAlNi γ_1' (2H) or Ni–Al (3R), in which each habit plane variant is composed of two correspondence variants, the model should be modified. In particular, the modeling would require both the existing HPV grouping system and a subgrouping structure for the CVs that comprise each HPV to enable deformation products (a single CV as opposed to a single HPV) to be accurately achieved. In addition, NiTi (B19′), the most commonly used SMA, even has a more complicated grouping structure as discussed later. The modification to the grouping structure to account for the difference between HPVs and CVs is currently being examined and will be presented elsewhere.

Three different materials are used in part 1 and they are CuZnAl, CuAlNi and NiTi. The parameters for each are listed in Table 1a. The set of crystallographic data for $Cu_{75}Zn_{17}Al_8$ (wt.%) was determined by Saburi and Wayman (Chakravorty and Wayman, 1979) and the lattice parameters of it were measured by Chakravorty and Wayman et al., (1977). The set for a Cu–14.2Al–4.3Ni (wt.%) alloy were calculated by Okamoto et al., 1974 and lattice parameters were measured by Otsuka and Shimizu (Otsuka and Shimizu, 1974). Finally, the set of crystallographic data and lattice parameters for a Ni–45.1Ti (wt.%) (Ni–50.2Ti at%) were both from Matusmoto et al., (1987). The crystallographic parameters can be used to obtain the transformation strains by

$$\varepsilon^{\text{tr}}_{ij} = \frac{1}{2} g(n_i m_j + n_j m_i) \tag{10}$$

The calculated transformation strains for $Cu_{75}Zn_{17}Al_8$ (wt.%) is shown in Table 1b. The grouping structure for this material is that four HPVs form a group clustering

Table 1(a)
Parameters of different materials used in simulation

Materials (wt.%)	$\hat{\mathbf{n}}$ $\hat{\mathbf{m}}$ (g)	μ (Gpa) ν[a]	B ($MPaK^{-1}$) F^C (MPa)	used in
$Cu_{75}Zn_{17}Al_8$	0.200, 0.705, 0.680 0.182, 0.641,−0.746 0.19	40 0.3	0.7 3.5[b]	Part 1 and 2
Cu–14.2Al–4.3Ni (type I)	− 0.2572, 0.6497, 0.7154 −0.1773,−0.7794, 0.6010 0.09589	35 0.3	0.11; 0.56[c]	Part 1
Cu–14.2Al–4.3Ni (type II)	0.2598, 0.7275, 0.6350 0.1299,−0.7015, 0.7007 0.09320	35 0.3	0.11; 0.56[c]	Part 1
Ni–45.1Ti	-0.8889,-0.2152, 0.4044 0.4144,−0.7633, 0.4981 0.13078	32 0.3	0.7 3.5[b]	Part 1
$Cu_{70}Zn_{26}Al_4$	−0.1489 0.7223, 0.6754 −0.1350, 0.6550,−0.7434 0.19386	40 0.3	0.7 3.5[b]	Part 2

[a] From Otsuka and Wayman (1998).
[b] From Patoor et al. (1994).
[c] Tailored from Shield (1995).

about one {110} type pole, and there are totally six such groups (Saburi and Wayman, 1979; Saburi et al., 1980). Unless explicitly mentioned all the calculations in part 1 are using the parameters in Table 1b.

3.2. Consideration of different martensite plates geometry

In a previous paper (Huang and Brinson, 1998), the single crystalline SMA model just described was demonstrated to exhibit the basic phenomenon of single crystalline SMA, such as the hysteresis loops of temperature induced transformation, and pseudoelasticity and the shape memory effect. However, the predictions of critical transformation stresses were higher than realistic. In this section we will investigate the effect of penny shaped martensite plates on model predictions and see how the transformation stress level can be reduced effectively.

The thin martensitic plates that appear in SMAs are better approximated by a penny-like inclusion rather than the spherical inclusion used previously. As we move away from convenient spherical symmetry the orientation of the inclusions must be modeled appropriately. Here, we will use a penny shaped inclusion ($a_1 = a_2 >> a_3$) for the group of habit plane variants (Fig. 5) and the choice of the n_3 axis is what must be determined. During thermally induced martensitic transformation, two strain accommodation steps occurred: (1) invariant plane strain due to the existence of the habit plane which almost eliminates the distortion strains, leaving small shear strains only; (2) self-accommodation by grouping together two or more favorable HPVs, further reducing shear strains to almost zero. For all martensitic structures

Table 1(b)
Transformation strains for $Cu_{75}Zn_{17}Al_8$ (wt.%)

Group	Variant	ε_{11}	ε_{22}	ϵ_{33}	γ_{23}	γ_{31}	γ_{12}
1	1	0.007	0.086	−0.096	−0.017	−0.005	0.049
	2	0.007	−0.096	0.086	−0.017	0.049	−0.005
	3	0.007	0.086	−0.096	−0.017	0.005	−0.049
	4	0.007	−0.096	0.086	−0.017	−0.049	0.005
	Average	0.007	−0.005	−0.005	−0.017	0.000	0.000
2	5	0.086	0.007	−0.096	−0.005	0.017	−0.049
	6	−0.096	0.007	0.086	0.049	0.017	0.005
	7	0.086	0.007	−0.096	0.005	0.017	0.049
	8	−0.096	0.007	0.086	−0.049	0.017	−0.005
	Average	−0.005	0.007	−0.005	0.000	0.017	0.000
3	9	0.007	0.086	−0.096	0.017	−0.005	−0.049
	10	0.007	−0.096	0.086	0.017	0.049	0.005
	11	0.007	0.086	−0.096	0.017	0.005	0.049
	12	0.007	−0.096	0.086	0.017	−0.049	−0.005
	Average	0.007	−0.005	−0.005	0.017	0.000	0.000
4	13	−0.096	0.007	0.086	0.049	−0.017	−0.005
	14	0.086	0.007	−0.096	−0.005	−0.017	0.049
	15	−0.096	0.007	0.086	−0.049	−0.017	0.005
	16	0.086	0.007	−0.096	0.005	−0.017	−0.049
	Average	−0.005	0.007	−0.005	0.000	−0.017	0.000
5	17	0.086	−0.096	0.007	−0.005	−0.049	0.017
	18	−0.096	0.086	0.007	0.049	0.005	0.017
	19	0.086	−0.096	0.007	0.005	0.049	0.017
	20	−0.096	0.086	0.007	−0.049	−0.005	0.017
	Average	−0.005	−0.005	0.007	0.000	0.000	0.017
6	21	−0.096	0.086	0.007	0.049	−0.005	−0.017
	22	0.086	−0.096	0.007	−0.005	0.049	−0.017
	23	−0.096	0.086	0.007	−0.049	0.005	−0.017
	24	0.086	−0.096	0.007	0.005	−0.049	−0.017
	Average	−0.005	−0.005	0.007	0.000	0.000	−0.017

except B19′, four HPVs tend to cluster about a {110} type pole and form a self accommodating group, as shown in Fig. 1–4. From Figs. 1–3, we see that the normals to each of the four habit plane in a given group are very close to the {110} pole direction about which the four variants cluster: therefore the n_3 direction will be taken as the appropriate {110} type pole direction for each of the self-accommodated groups in the model. The direction of the symmetric axis is decided by angles θ (rotation with respect to axis x_3) and ϕ (rotation with respect to axis x_2).

The comparison of the stress–strain curve of shape memory effect for both spherical martensite plates and penny-shaped martensite plates is shown in Fig. 6. The critical transformation stress is greatly reduced in the case of penny-shaped martensite

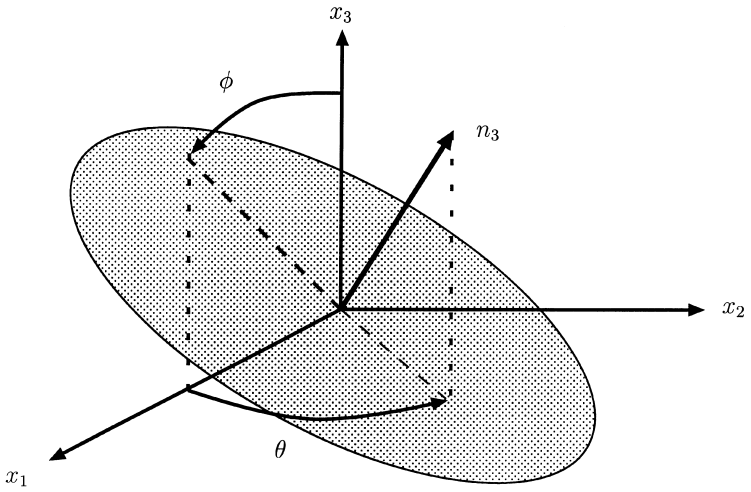

Fig. 5. The orientation of a penny-shaped martensite plate relative to austenite material axes x_1, x_2, and x_3. Normal, n_3, is parallel to smallest dimension of penny ($a_1 = a_2 > > a_3$).

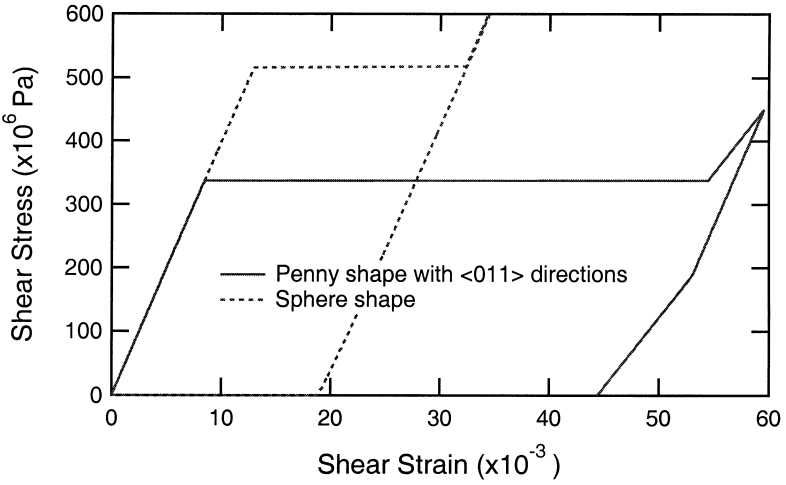

Fig. 6. Comparison of the stress–strain curve of shape memory effect for spherical and penny-shaped assumption of martensite plates. In these two cases, all factors are the same except the shape of martensite plates is different.

plates since the interaction energy with respect to a penny shape inclusion is much lower than that for a spherical shape.

4. Results

In this section, we will explore the impact of specific crystallographic details on the overall stress-strain response as predicted by the multivariant model. We will

consider the orientation dependence of load, type I vs. type II twins, effect of loading mode and the self-accommodated group structure.

Note that throughout this section, the model as described in the previous section is used. This necessitates that the grouping structure used is one with a single grouping hierarchy (G groups of V habit plane variants) and no additional sub-grouping structure for CVs is included. Thus, there is automatically an approximation involved for the comparisons with results for NiTi and CuAlNi materials. Nevertheless, we believe the current analysis provides useful qualitative information without the additional level of complexity. Indeed, this type of simulation will indicate whether the sub-grouping details impact overall response sufficiently to merit further study.

4.1. Orientation dependence and twin types

Uniaxial tension experiments were performed on three single crystal specimens of Cu–13.95Al–3.93Ni (wt.%) by Shield (1995). Specimen T1 had a tensile axis of [2.43 1 0]; T2 was oriented 15° from [1 1 1] direction and had a [1 1 1.73] tensile axis direction; T3 had the [1 1 1] direction as its tensile axis. The Ms and As have same value of 3.9°C and the experiment was performed at temperature 40°C. The results of these experiments are shown in Fig. 7.

There are several notable features of these results. First, we see that the initial moduli of all the specimens differ, as do the transformation stresses. Specimen T1 has the lowest initial modulus, T3 the largest one, and T2 an intermediate modulus. The difference in the initial modulus is consistent with the behavior of a cubic crystal. Compliance of a cubic crystal can be expressed as (Nye, 1985)

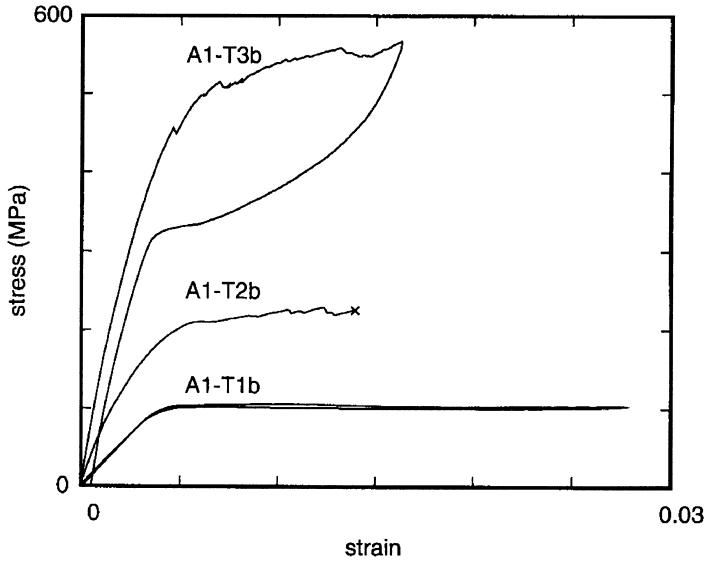

Fig. 7. The stress–strain curves for fully austenitic specimens A1–T1b, A1-T2b and A1–T3b at 40°C. (Ms + As)/z is 3.9°C (after Shield, 1995).

$$S = S_{11} - 2(S_{11} - S_{12} - \tfrac{1}{2}S_{44})(l_1^2 l_2^2 + l_2^2 l_3^2 + l_3^2 l_1^2) \tag{11}$$

where S is the compliance in direction $[l_1\ l_2\ l_3]$, S_{11}, S_{12}, and S_{44} are the corresponding elements in the abbreviated matrix of the 4th order compliance tensor S_{ijkl}. For a CuAlNi shape memory alloy, since $S_{11} - S_{12} - \frac{1}{2}S_{44}$ is greater than zero (Hellwege and Magdelung, 1984), the maximum compliance is in the $<1\,0\,0>$ direction, i.e. $S_{max} = S_{11}$. Meanwhile, the minimum compliance is in the $<1\,1\,1>$ direction, i.e. $S_{min} = S_{11} - \frac{2}{3}(S_{11} - S_{12} - \frac{1}{2}S_{44})$. As a result of the inverse relationship between the compliance and Young's modulus, the maximum Young's modulus is in the $<1\,1\,1>$ direction and minimum in the $<1\,0\,0>$ direction. The trend for magnitude of the transformation stress is similar to the trend in the initial moduli (Shield, 1995). That is, the specimen T1 ([2.43 1 0] direction) has the lowest transformation stress and the specimen T3 ([1 1 1] direction) has the largest transformation stress.

In order to verify the applicablility of the single crystal model, we calculated three tensile loading and unloading cases with exactly the same orientations as those appeared in Shield's experiments. We use the habit plane normals calculated by Okamoto et al. (1986) who used the lattice parameters in a Cu–14.2Al–4.3Ni (wt.%) alloy measured by Otsuka and Shimizu (1974). In the simulation T_0 is set to equal to (Ms + As)/2, i.e. 3.9°C and $T = 40$°C. Other parameters we used are listed in Table 1a. The result of our prediction is shown in Fig. 8.

It is observed that different tension direction leads to different transformation stresses in our simulation which agrees with the experimental results shown in Fig. 7. Moreover, the sequence of these transformation stresses is also similar to that found in the experiment, that is, tension in [1 1 1] has the highest transformation stress, and tension in [2.43 1 0] has the lowest one. Fig. 7 showed that the transformation stresses have a maximum to minimum ratio of 4.9, and that predicted by our model

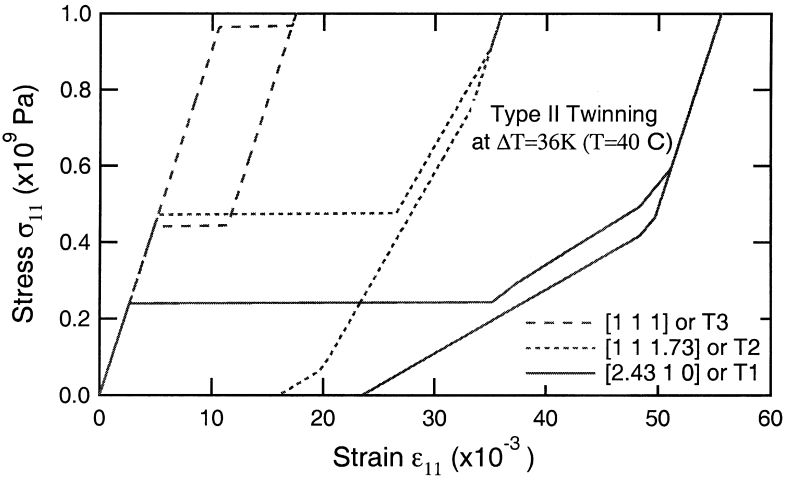

Fig. 8. Model predicted results for a Cu–14.2Al–4.3Ni (wt.%) alloy under different uniaxial loading directions. The temperature is set to be $\Delta T = 36$K and type II twinning is used as the lattice invariant shear.

is 4.0. This shows that our model is consistent with the main trends of stress–strain relationship in SMAs. In addition we also examined here the choice of a different twinning type in the model. We simulated the same set of experiments, using the same material lattice parameters but with type I twinning (Fig. 9). It is seen that the results are similar to those using type II twinning. However, the ratio of the maximum transformation stress to the minimum for type I is 3.6, and none of three curves shows pseudoelasticiy effect. In the case of type II twinning, T3 shows pseudoelasticity effect and T2 shows some reverse transformation. Thus, the single crystal model appears to be accurately capturing macroscopic differences due to microstructural twinning type. Although these results are not conclusive due to the approximation in the grouping, the results strongly indicates that crystallographic details are important to the overall macroscale modeling, a fact also pointed out by Gall et al. (1998).

In spite of these encouraging results, the model predictions still have some discrepancies with the experimental results. First, the magnitude of transformation stress is still nearly double that of the experimental result. Furthermore, Shield (1995) showed the Young's moduli at 40°C are 26.7, 72.0, and 158 GPa, respectively. This leads to a maximum to minimum ratio of 5.9. In our simulation, the ratio is 1 because we assumed both austenite and martensite are isotropic and have the same elastic constants.

4.2. Anisotropy effects

We believe the assumption of isotropy for the matrix phase in the single crystal model is responsible for some significant discrepancies in predictive results due to the large anisotropy factor of austenite and martensite in SMAs. Since most single crystals of shape memory alloys have a cubic structure (Funakubo, 1987) three

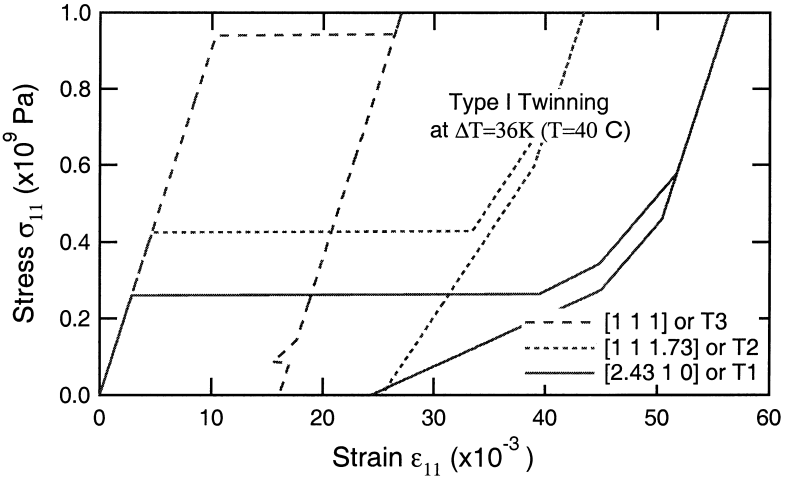

Fig. 9. Model predicted results for a Cu–14.2Al–4.3Ni (wt.%) alloy under different uniaxial loading directions. The temperature is set to be $\Delta T = 36$K and type I twinning is used as the lattice invariant shear.

independent elastic constants, i.e. S_{11}, S_{12}, and S_{44} (or C_{11}, C_{12}, and C_{44}) (Nye, 1985) are usually needed to express the 4th order compliance or stiffness tensor. For example, a typical set of C_{11}, C_{12}, and C_{44} for a Cu–14Al–4.1Ni (wt.%) alloy quenched in 0°C water (Hellwege and Magdelung, 1984) is 142.6, 127.4 and 97 GPa. The anisotropy factor in the cubic system is defined as

$$A = C_{44}/\tfrac{1}{2}(C_{11} - C_{12}) \tag{12}$$

Thus, the anisotropy factor is 12.8 for this alloy. For an isotropic material, since $C_{44} = \frac{1}{2}(C_{11} - C_{12})$, the anisotropy factor is always 1. The corresponding set of S_{11}, S_{12}, and S_{44} in the same previous alloy is 44.5,−21.0 and 10.3 $(\text{TPa})^{-1}$. Using Eq. (11), we find that $S_{max} = S_{11} = 44.5\ (\text{TPa})^{-1}$, $S_{[2.43\ 1\ 0]} = 29.55\ (\text{TPa})^{-1}$, $S_{[1\ 1\ 1]} = S_{min} = 4.27\ (\text{TPa})^{-1}$. The ratio of S_{max} to S_{min} is 10.4 and that of $S_{[2.43\ 1\ 0]}/S_{[1\ 1\ 1]}$ is 6.9. The latter is also the theoretical ratio of Young's modulus along these two tension directions which agrees well with the ratio of 5.9 in Shield's experiment.

From this discussion, it is apparent that the strong anisotropy of austenite should be accounted for in modeling. Such a modification would then properly reflect the different initial moduli and would impact the transformation stresses as is illustrated by results in the next section. Since there is no closed form Eshelby Tensor for anisotropic Eshelby inclusion problem, this modification is not trivial and numerical techniques are being considered. Given this major discrepancy between the current model and the material the comparison between Figs. 7 and 8 is quite encouraging and acceptable.

To follow up on our hypothesis that the anisotropy of the single crystal could play an important role in the transformation stress levels, here we simulate the response

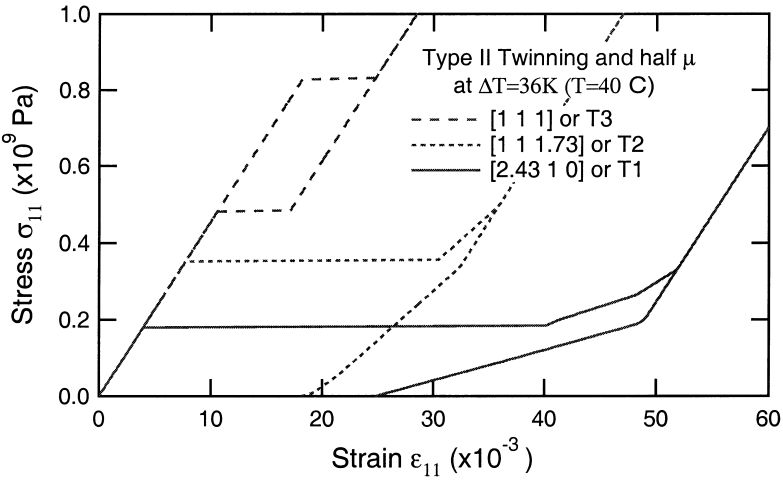

Fig. 10. Model predicted results for a Cu–14.2Al–4.3Ni (wt.%) alloy under different uniaxial loading directions. The temperature is set to be $\Delta T = 36$K, type II twinning is used as the lattice invariant shear and the shear modulus is reduced by half.

of the same material with type II twinning, but we reduce our isotropic austenitic matrix shear modulus by a factor of 2. As can been seen in Fig. 10, all three transformation stresses are lowered by 14, 25 and 25%, respectively, since in our model higher moduli corresponds to higher interaction energy. It is also interesting to note that in the polycrystal material simulation (described in Part 2), the same reduction in μ by 2 results in over a 26% decrease in macroscopic transformation stress for uniaxial tension. Since there are many differently oriented grains in a polycrystal specimen, many of them will be oriented with a lower modulus direction parallel to the loading axis.

4.3. Stress state variations

In addition to the anisotropy exhibited by SMA materials, tension/compression asymmetry has also been shown (Patoor et al., 1995; Shield, 1995; Gall et al., 1998). Our model can capture this asymmetry since it is due to activation of different variants with different loading modes. In Part 2 of this paper, we will be making comparison to experimental data for a polycrystalline material response to multiaxial loading states. It is instructive to first consider the response of the single crystal material subjected to the same loading states. Fig. 11 shows the curves of effective transformation stresses vs. effective transformation strains for $Cu_{75}Zn_{17}Al_8$ (wt.%) single crystal subjected to the first six different loading states (exact tabulation given in Part 2 of this paper). The seventh loading state of pure hydrostatic compression is not considered since pure hydrostatic stress showed no transformation. In Fig. 12, the trend of effective transformation stress at 100% transformation vs. hydrostatic pressure at 100% transformation is shown. The results show that the effective transformation stress tends to decrease with increasing hydrostatic pressure. These model results are

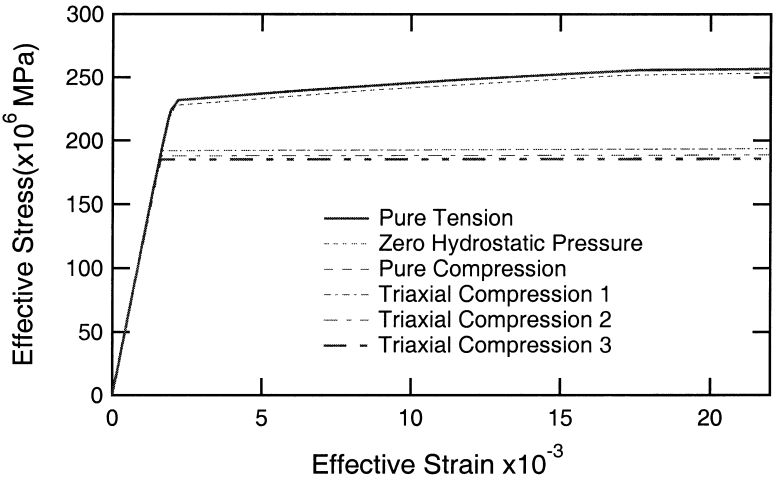

Fig. 11. Model predicted effective stress–strain curves for a CuZnAl single crystal under different uniaxial and triaxial loading states (see Part 2 for description).

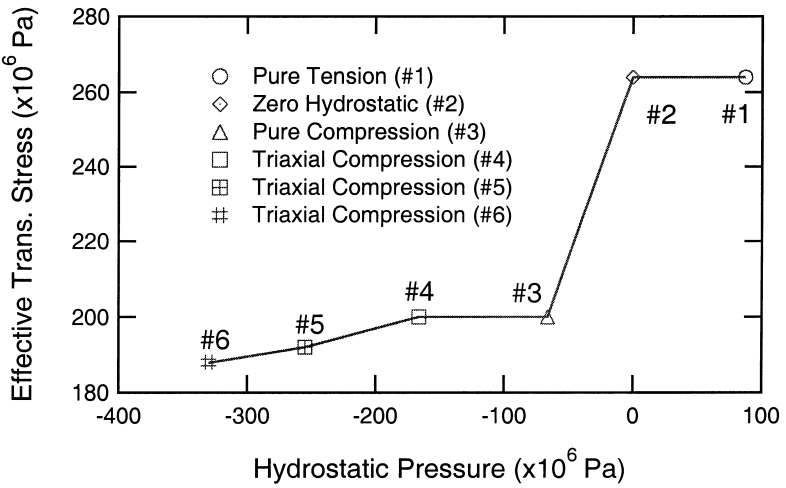

Fig. 12. Model predicted effective stress at 100% transformation vs. hydrostatic pressure at 100% transformation for a CuZnAl single crystal under different uniaxial and triaxial loading states.

consistent with the thermodynamically based continuum transformation criteria (Sun and Hwang, 1991; Boyd and Lagoudas, 1996), i.e. increasing hydrostatic pressure raises the effective stress at transformation for materials with positive volume change and lowers it for materials with negative volume change. The irregularities in the trend of Fig. 12 are likely due to the fact that the transformation of martensite is a competition between hydrostatic pressure and microscopic characteristics of martensitic transformation. Gall et al. (1998) hypothesized that there were more variants available which transform faster in certain cases. Further discussion on multiaxial loading is given in Part 2 of this paper.

4.4. Effect of grouping possibilities for NiTi

In previous sections, the self-accommodation groups for 18R (9R) and 2H SMAs have been discussed. NiTi (B19′) SMA, however, has a more complicated self-accommodating grouping structure (Miyazaki et al., 1989a,b). The martensitic self-accommodating groups in a Ti–Ni alloy exhibit a triangular morphology consisting of three habit plane variants, while each habit plane variant is composed of two correspondence variants as in Fig. 14. While only three HPVs appear at a time in a particular plate, as before the variants can be divided into symmetric clusters of four HPVs about pole directions: for a given cluster of four HPVs, there are four possible sets of three that can appear in a physical plate structure. For the structures examined previously (3R, 2H, 18R) a given HPV could only appear in one given self-accommodated grouping (we term this "exclusive grouping"). For NiTi however, the grouping structure is "non-exclusive" and complicates modeling. We have examined here several modeling possibilities, with emphasis on artificial merging of observed groups for simplification.

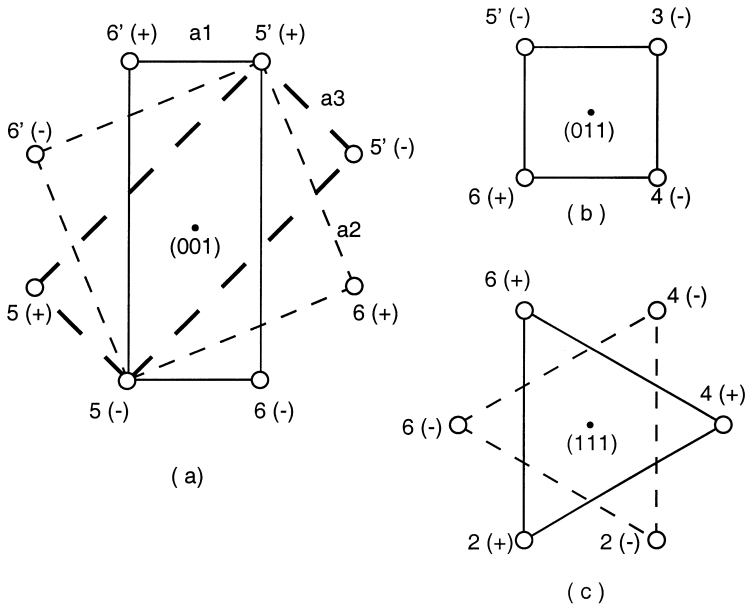

Fig. 13. Schematic drawing showing how different grouping methods are possible for NiTi SMAs: (a) HPVs clustering about (001) pole, (b) HPVs clustering about (011) pole, and (c) HPVs clustering about (111) polea (after Miyazaki et al., 1989a,b).

The HPVs in NiTi do not cluster as tightly about pole directions as the earlier structures, leading to a number of possible interpretations for appropriate plate groupings. Miyazaki et al. (1989a,b) mention possible self-accommodation by clustering habit plane variants about anyone of the {001}, {011} and {111} poles relative to the parent phase. As shown in Fig. 13, there are two possibilities for pole {111} in (c). One is that three habit plane variants form a self-accommodating group designated by the solid triangle, the other is that all the six habit plane variants form a self-accommodating group. For pole {011} in (b), the only possibility is all the four habit plane variants together form one group. However, for pole {001} in (a) there are three different methods to form four variant groups, which are distinguished by solid rectangle, light dashed rectangle and heavy dashed rectangle, and one method to form a group consisting of all eight habit plane variants. Note that Fig. 13 shows only one of the crystallographically equivalent groups in each case: for example, the a1 grouping scheme is depicted as variants $6'(+)$, $5'(+)$, $6(-)$, $5(-)$; in addition to these four HPVs, there are five other crystallographically equivalent sets of four HPVs forming six groups in total (for 24 HPVs). For a1, there are two sets of four HPVs about each {001} type pole, where in Fig. 13a $6'(-)$, $5'(-)$, $6(+)$, $5(+)$ is the equivalent group not highlighted for clarity.

In Table 2, we go through possible self-accommodating groups, mention whether each is observed experimentally, explore the results predicted by the Multivariant model using simplified grouping morphology and discuss improvements needed in the model in order to fully reflect this sophisticated self-accommodating structure.

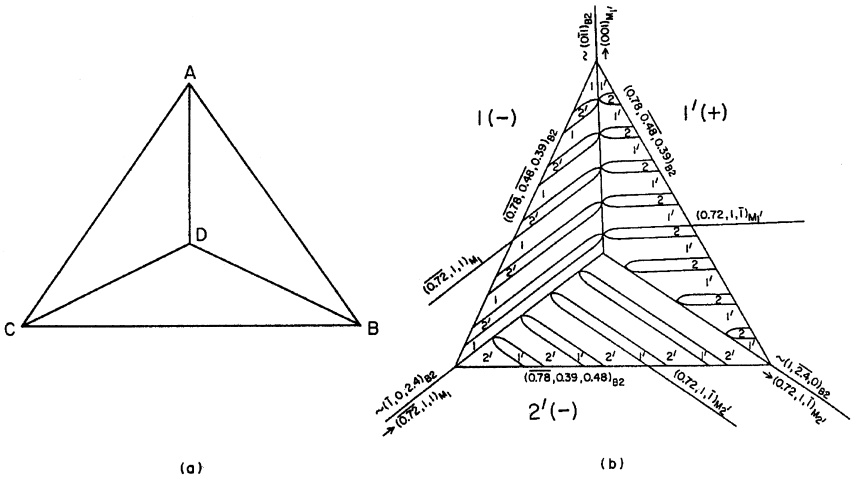

Fig. 14. (a) Schematic drawing of triangular martensite morphology, and (b) sub-micro model depicting crystallographic relations between variants in the triangular morphology (after Miyazaki et al., 1989a,b). Normal, n_3, is out of paper.

We calculated the transformation stress under pure shear for most of the possible self-accommodating groups. Here we use the habit plane normals with a type II twinning mode calculated by Matsumoto et al. (1987) for a Ti-49.8Ni (at. %) SMA. Other parameters we used are listed in Table 1a. As shown in Fig. 14b, for a real three HPV self-accommodating group the three habit planes (three sides of the triangle) are almost parallel to the paper since they cluster about one of {001} type pole. Therefore, the dimension of this self-accommodating group vertical to the paper is the smallest, and this direction is chosen as the n_3 direction for the model calculations. For the simulations using groups of four or eight HPVs, the n_3 direction remains the same since all the self-accommodating groups being merged cluster about the same pole.

Note that for a1 and a2 we do not sub-divide each of the six groups into the four possible sets of three HPVs to represent the experimentally observed triangular morphology shown in Fig. 14. a1 and a2 as they occur in the material are non-exclusive groupings and can in fact appear simultaneously: we choose here to approximate with a much simpler artificial merging as exclusive groupings (see Table 2) and only allow one grouping scheme at a time to appear. In addition, in each case the simulation considers the habit plane variants as the smallest sub-unit, not accounting for the finely twinned CVs which make up each HPV. The transformation stress values obtained are high, but the relative ordering indicates that some grouping structure is needed and that artificial merging may be a useful modeling simplification tool for NiTi. While the clustering of four habit plane variants about a {011} pole, grouping b, is the only suitable accommodation for most other long-period stacking order structures, for example 18R (9R) and 2H, it is not observed experimentally for NiTi (Miyazaki et al., 1989a,b). The {111} pole groupings and a3 for the {001} pole are also not seen experimentally (Miyazaki et al., 1989a,b). Other papers in the

Table 2
Single crystal model predicted transformation stress under pure shear for different possible self-accommodating groups[a]

Clustering pole	Possible crystallographically independent self-accommodating group from Fig. 13	Actual morphology of plate group	Simulated morphology of plate group	Transformation stress under pure shear (MPa)
{001}	a1: solid line, four variants: 6′(+) 5′(+) 5(−) 6(−) (total of six such groups, two about each {100} type pole)	Four possible sets of three HPVs (from a1 group) form self-accommodating groups: • 6′(+) 5′(+) 5(−) • 6′(+) 5′(+) 6(−) • 6′(+) 5(−) 6(−) • 5′(+) 5(−) 6(−)	Four variants in one self-accommodating group: • 6′(+) 5′(+) 5(−) 6(−)	940
	a2: dashed line, four variants (total of six such groups)	Four sets of three HPVs (from a2 group) form self-accommodating groups	As one self-accommodating group	1210
	a3: heavy dash, four variants (total of six such groups)	Not observed	As one self-accommodating group	1550
	a4: eight variants (total of three such groups)	Not observed	As one self-accommodating group	940
{011}	b: four variants (total of six such groups)	Not observed	As one self-accommodating group	Not calculated
{111}	c1: three variants (total of eight such groups)	Not observed	As one self-accommodating group	Not calculated
	c2: six variants (total of four such groups)	Not observed	As one self-accommodating group	Not calculated

[a] Examples are for one set of variants only for simplicity — crystallographically equivalent groups also appear; the a1 example is shown in more detail than others.

literature have referred to these groupings however: the b grouping can be found in (Gall et al., 1999) and a3 in (Lu and Weng, 1998), although in both papers the groupings were not explicitly used in the model approximations. It is clear from the tabulation that the calculated transformation stresses from the multivariant model are too high. For the cases such as a3 where the product is not seen experimentally, the high predictions are not a great concern. For the a1 and a2 cases which are observed, the high stress predictions indicate that the model should be modified to more appropriately account for the complex morphology of NiTi. Possible solutions include allowing the proper representation of four possible sets of three HPVs in each group, and/or including the subgrouping on CVs. The complication of triangular morphology seems to be specific to NiTi, while the subdivision of HPVs into the finely twinned CVs is also key for 2H and 3R materials.

5. Conclusion

In this paper, we have extended the multivariant model for SMA response prediction to consider more realistic penny-shaped inclusions and we discuss the impact of several microscale features on macroscopic response predictions. The results here confirm that some details of the crystallography have significant influence on macroscale response and need to be captured by models. The following are the major results in this paper:

- Inclusion shape in the micromechanics model is important: penny-shaped inclusions reduced transformation stresses by a factor of 2.
- Grouping structure can greatly influence material response predictions: here we examined different choices for self-accommodated groups for a particular NiTi material and showed dramatic differences in transformation stresses. This result indicates a proper way to fully represent the self-accommodating structure (e.g. using 48 groups instead of artificial merging) as well as the distinction between HPV's and CVs should be examined in more detail in future work as they may play key roles in more accurate predictions.
- Since the multivariant model can capture activation of different variants, the effect of different loading modes (e.g. tension vs. compression) and effect of material orientation relative to loading axis are captured by the model.
- One major contributor to orientation dependence of material response is anisotropy of the crystal lattice. It is shown here that the level of anisotropy exhibited by SMAs requires future modeling changes to incorporate this feature.
- Twinning type is shown to significantly affect the material response and thus is important in initial calculation of parameters for use with any micromechanics model.

While the results here indicate that the Multivariant model is still maturing, the trends are promising and the findings point to two key areas for future model refinements. First, the anisotropy of the austenite single crystal needs to be accounted for: this change would impact not only initial slopes of stress-strain response, but also

magnitude of transformation stress, orientation dependence, and would have great impact on polycrystalline response. Secondly, the different results seen for several self-accommodated grouping structures for NiTi indicate that the more complicated sub-grouping structure inherent in 2H, 3R and B19′ shape memory materials should be further examined and included in the model. In addition, the results here have broader implications as to important considerations for other types of micromechanics SMA models as well as phenomenological models.

References

Barrett, C., Massalski, T.B., 1980. Structure of Metals: Crystallographic Methods, Principles and Data. Pergamon Press, Oxford.

Bilby, B.A., Crocker, A.G., 1965. The theory of the crystallography of deformation twinning. Proc. Roy. Soc. A, 288 (No. 1413), 240–255.

Bowles, J.S., Machenzie, J.K., 1954. The crystallography of martensite transformations I. Acta Metall. 2 (Jan.), 129–137.

Boyd, J.G., Lagoudas, D.C., 1996. A thermodynamical constitutive model for shape memory materials. Part I. The monolithic shape memory alloy. Int. J. Plast. 12 (6), 805–842.

Cahn, R.W., 1953. Plastic deformation of alpha-uranium; twinning and slip. Acta Metall. 1 (Jan.), 49–70.

Chakravorty, S., Wayman, C.M., 1977. Electron microscopy of internally faulted Cu–Zn–Al martensite. Acta Metall. 25, 989–1000.

Crocker, A.G., 1965. Deformation Twinning. Gordon & Breach, New York.

Funakubo, H., 1987. Shape Memory Alloys. Gordon and Breach Science Publishers, New York.

Gall, K., Sehitoglu, H., Maier, H.J., Jacobus, K., 1998. Stress-induced martensitic phase transformations in polycrystalline CuZnAl shape memory alloys under different stress states. Metall. Trans. A 29A (Mar.), 765–773.

Gall, K., Sehitoglu, H., Chumlyakov, Y.I., Kireeva, I.V., Maier, H.J., 1999. The influence of aging on critical transformation stress levels and martensite start temperature in NiTi: part I, aged microstructure and micro-mechanical modeling. J. Eng. Mater. Tech. (special edition on Shape Memory Alloy), 121 (Jan.), 19–27.

Hellwege, K.-H., Magdelung, O. 1984. Numerical Data and Functional Relationships in Science and Technology: New Series: Group III: Crystal Solid State Physics: Elastic and Piezoelectric, Pyrelectric, Peizooptic, Electrooptic Constants, Nonlinear Dielectric Susceptibilities of Crystals, Vol. 18. Springer-Verlag, New York.

Huang, M., 1997. A Multivariant Model for Shape Memory Alloys. Mechanical Engineering, Northwestern University, Evanston, IL.

Huang, M.S., Brinson, L.C., 1998. A Multivariant Model for Single Crystal Shape Memory Alloy Behavior. J. Mech. Phys. Solids 46 (8), 1379–1409.

Knowles, K.M., Smith, D.A., 1981. The crystallography of the martensitic transformation in equiatomic Nickel–Titanium. Acta Metall. 29, 101–110.

Lexcellent, C., Goo, B.C., Sun, Q.P., Bernardini, J., 1996. Characterization, thermomechanical behavior and micromechanical-based constitutive model of shape-memory Cu–Zn–Al single crystals. Acta Mater. 44 (9), 3773–3780.

Lu, Z.K., Weng, G.J., 1997. Martensitic transformation and stress–strain relations of shape-memory alloys. J. Mech. Phys. Solids 45 (11/12), 1905–1928.

Lu, Z.K., Weng, G.J., 1998. A self-consistent model for the stress–strain behavior of shape-memory alloy polycrystals. Acta Metall. 46 (15), 5423–5433.

Matsumoto, O., Miyazaki, S., Otsuka, K., Tamura, H., 1987. Crystallography of martensitic transformation in Ti–Ni single crystals. Acta Metall. 35 (8), 2137–2144.

Miyazaki, S., Otsuka, K., Wayman, C.M., 1989a. The shape memory mechanism associated with the martensitic transformation in Ti–Ni alloys II. Variant coalescence and shape recovery. Acta Metall. 37 (7), 1885–1890.

Miyazaki, S., Otsuka, K., Wayman, C.M., 1989b. The shape memory mechanism associated with the martensitic transformation in Ti–Ni alloys I. Self-accommodation. Acta Metall. 37 (7), 1873–1884.

Mura, T., 1987. Micromechanics of Defects in Solids. Kluwer Academic Publishers, Boston.

Murakami, Y., Otsuka, K., Hanada, S., Watanabe, S., 1994. Self-accommodation and morphology of 14M (7R) martensites in a Ni–37.0at.%Al alloy. Mater. Sci. Eng. A189, 191–199.

Nye, J.F., 1985. Physical Properties of Crystals: Their Representation by Tensors and Matrices. Clarendon Press, Oxford.

Okamoto, K., Ichinose, S., Morii, K., Otuska, K., Shimizu, K., 1986. Crystallography of β'_1 to γ'_1 stressed-induced martensitic transformation in a Cu–Al–Ni alloy. Acta Metall. 34 (10), 2065–2073.

Otsuka, K., Shimizu, K., 1974. Morphology and crystallography of thermoelastic Cu–Al–Ni martensite analyzed by the phenomenological theory. Trans. JIM 15, 103–108.

Otsuka, K. and Wayman, C.M., 1998. Shape Memory Materials. Cambridge University Press, New York.

Otsuka, K., Ohba, T., Tokonami, M., Wayman, C.M., 1993. New description of long period stacking order structures of martensites in β-phase alloys. Scr. Metall. 29, 1359–1364.

Patoor, E., Eberhardt, A. and Berveiller, M. 1994. Micromechanical modelling of the shape memory behavior. In: Proc. ASME International Congress and Exposition, AMD-vol. 189, 23–27, Chicago.

Patoor, E., Amrani, M.E., Eberhardt, A., Berveiller, M., 1995. Determination of the origin for dissymetry observed between tensile and compression tests on shape memory alloys. J. Physique IV 5 (C2), 495–500.

Reed-Hill, R.E., Abbzachian, R., 1992. Physical Metallurgy Principles. PWS-Kent Publishing Company, Boston.

Saburi, T., Nenno, S., 1981. The shape memory effect and related phenomena. Proc. An International Conference on Solid to Solid Phase Transformations, pp. 1455–1479.

Saburi, T., Wayman, C.M., 1979. Crystallographic similarities in shape memory martensites. Acta Metall. 27, 979–995.

Saburi, T., Nenno, S., Kato, S., Takata, K., 1976. Configurations of martensite variants in Cu–Zn–Ga. J. Less Common Metals 50, 223–236.

Saburi, T., Wayman, C.M., Takata, K., Nenno, S., 1980. The shape memory mechanism in 18R martensitic alloys. Acta Metall. 28, 15–32.

Shield, T.W., 1995. Orientation dependence of the pseudoelastic behavior of single crystals of Cu–Al–Ni in tension. J. Mech. Phys. Solids 43 (6), 869–895.

Sun, Q.P., Hwang, K.C., 1991. A micromechanics constitutive model of transformation plasticity with shear and dilatation effect. J. Mech. Phys. Solids 39, 507–524.

Sun, Q.P., Zhang, X., Xu, T.T., 1997. Some recent advances in experimental study of shape memory alloys. In: Proc. IUTAM Symposium on Macro- and Micro-Aspects of Thermoplasticity, vol. 62, 407–416, Bochum, Germany.

Sun, Q.P., Xu, T.T., Zhang, X., 1999. On deformation of A–M interface in single crystal shape memory alloys and some related issues. Tran. ASME 121 (Jan.), 38–43.

Wechsler, M.S., Lieberman, D.S., Read, T.A., 1953. On the theory of the formation of martensite. Trans AIME 197, 1503–1515.